

# Origins of Fermi Surfaces, Pseudogap and High Temperature Superconductivity in Copper Oxide Superconductors

Hiroshi Kamimura<sup>1\*</sup>, Jaw-Shen Tsai<sup>1,2</sup>, Osamu Sugino<sup>3</sup>, Kunio Ishida<sup>4</sup>, Hideki Ushio<sup>5</sup>

1. *Tokyo University of Science, 1-3 Kagurazaka, Shinjuku-ku, Tokyo, 162-8601, Japan.*

2. *RIKEN Center for Emergent Matter Science (CEMS), Wako, Saitama 351-0198, Japan*

3. *University of Tokyo, Institute of Solid State Physics, 5-1-5 Kashiwanoha, Kashiwa, Chiba, 277-8581, Japan.*

4. *Corporate Research and Development Center, Toshiba Corporation 1 Komukaitoshiba-cho, Saiwai-ku, Kawasaki 212-8582, Japan.*

5. *Tokyo National College of Technology, Hachioji, 193-0997, Japan.*

In this paper, we clarified the origins of the pseudogap and the mechanism of d-wave superconductivity in copper oxide (cuprate) superconductors. Paying attention to the unusual property of cuprates, i.e. a deformation in the opposite direction to the Jahn-Teller distortion by doping holes, called the anti-Jahn-Teller effect, we show theoretically that the electronic structure of copper oxides changes drastically upon doping holes, and thus that the Fermi surface structure of  $\text{La}_{2-x}\text{Sr}_x\text{CuO}_4$  (LSCO), the simplest copper oxide, consists of Fermi pockets in antinodal regions and Fermi arcs in nodal regions in the underdoped region. Moreover, the novel particles on the Fermi pockets contribute to the phonon mechanism in d-wave superconductivity.

PACS numbers: 74.25.Jb, 74.20.Mn, 74.72.-h, 79.60.-i

Thirty years have passed since the discovery of high temperature superconductivity in cuprates [1], but a consensus on its physical origin has not yet been reached [2]. The purpose of this Letter is to break this deadlock, paying special attention to the unusual properties of cuprate superconductors that most of models have ignored, such as the anti-Jahn-Teller (JT) effect [3] and the randomness caused from doping chemical elements or making oxygen deficiencies, and thus, to clarify the origins of pseudogap [2] and the mechanism of d-wave superconductivity [4].

During the past thirty years, the clarification of Fermi surface structures was a central issue. There were two views. One view was based on the single-component theory of the t-J model [5], which predicts that a metallic state has a large Fermi surface (FS) near the optimal hole doping. Since angle-resolved photoemission spectroscopy (ARPES) experiments did not show the portion of a large FS, the opening of an energy gap near the antinodal region (pseudogap) was suggested [6]. An alternative view was based on the two-component theory [7], in which a doped hole forms a metallic state, by taking alternately the two types of orbital states in the local antiferromagnetic (AF) order without destroying the AF order. As a result, small Fermi pockets are constructed by doped holes. This model is called the K-S model [8], which are based on the two key factors: (i) the electron correlation [9], and (ii) the anti-Jahn-Teller (JT) effect.

The energy separation between the two types of orbital states, which were originally split by the JT effect, becomes smaller upon doping holes, as a result of the anti-JT effect. These orbital states are named as an  $a_{1g}$  antibonding orbital  $|a_{1g}^* \rangle$  and a  $b_{1g}$  bonding orbital  $|b_{1g} \rangle$  in a  $CuO_6$  octahedron, which are shown in Fig. 1(a). This anti-JT effect were supported experimentally [10-12], and by the band calculations including the electron-correlation effect [13].

In Fig. 1(b), the K-S model are explained for LSCO in a heuristic manner using an extended two-story-house model. The unique feature of the K-S Hamiltonian to describe the K-S model (see Eq. (1) of Ref. [14]) lies in the exchange interactions between the spin of a doped hole  $s_{im}$  ( $m = a_{1g}^*$  or  $b_{1g}$ ) and that of a localized hole  $S_i$  in the  $b_{1g}$  antibonding orbitals  $|b_{1g}^* \rangle$  within the  $i$ -th  $CuO_6$  octahedron (the same Cu house in Fig. 1(b)), given by

$$H_{ex} = \sum_i (K_{a^*1g} s_{i,a^*1g} \cdot S_i + K_{b1g} s_{i,b1g} \cdot S_i). \quad (1)$$

Here  $K_{a^*1g}$  and  $K_{b1g}$ , are the exchange constants for the Hund's coupling

spin-triplet and spin-singlet (SS) states, respectively, and their numerical values for a CuO<sub>6</sub> octahedron in LSCO are  $K_{a^*1g} = -2.0$  eV and  $K_{b1g} = 4.0$  eV [15].

Using the K-S Hamiltonian, the energy bands in underdoped LSCO was calculated by treating  $H_{\text{ex}}$  in the mean-field approximation [16], which replaces the localized spins  $S_i$  in Eq. (1) with their average value  $\langle S \rangle$ . The  $|K_{a^*1g}|$  and  $K_{b1g}$  in Eq. (1) are proportional, respectively, to the overlap between the  $|a^*_{1g}\rangle$  and  $|b^*_{1g}\rangle$  orbitals and that between the  $|b_{1g}\rangle$  and  $|b^*_{1g}\rangle$  orbitals. When holes are doped into the AF insulator, the apical-oxygen - Cu distance in CuO<sub>6</sub> octahedrons in LSCO decreases by the anti-JT effect, and thus, the overlap between  $|a^*_{1g}\rangle$  and  $|b^*_{1g}\rangle$  orbitals increases, resulting in the increase of  $|K_{a^*1g}|$  while  $K_{b1g}$  does not change.

In the previous energy-band calculations [16], a value of  $|K_{a^*1g}|$  was treated as a constant. In this context, a new method of improving the previous calculations is proposed in the present paper, where a value of  $|K_{a^*1g}|$  in Eq. (1) changes with the hole concentration  $x$ . Figure 2(a) shows the thus-calculated energy bands for  $x = 0.03$  below the metal-insulator transition  $x_0 = 0.05$ . In this case, doped holes enter the fully-occupied #1 band, the highest band, from its highest state at the  $\Delta$  point,  $(\pi/2a, \pi/2a)$ , a middle point on the side of a two-dimensional (2D) square Brillouin zone (BZ), which is obtained by projecting the ordinary (BZ) in Fig. 1(c) onto the  $k_x - k_y$  plane, where  $a$  is the length of the Cu-O-Cu distance.

When  $x$  increases to  $x_0 = 0.05$ ,  $|K_{a^*1g}|$  increases and the metal-insulator transition occurs. The energy bands thus calculated for the metallic phase are different from those for the insulating phase. Figure 2(b) shows the band structure calculated for  $x = 0.10$  in the underdoped regime between  $x_0 = 0.05$  and optimum doping  $x_{\text{optm}} = 0.15$ . The state at the  $G_1$  point  $(\pi/a, 0)$  becomes the highest state in the #1 band, in which the density of states (DOS) shows the saddle-point singularity at  $(\pi/a, 0)$ . Hereafter we take  $a$  as unity, so that  $\Delta$  and  $G_1$  points are expressed as  $(\pi/2, \pi/2)$  and  $(\pi, 0)$  in the text, respectively.

Now we discuss the features of the electronic states calculated for  $x = 0.03$  and  $x = 0.10$ , by investigating their wavefunctions in real space. The wavefunction at  $(\pi/2, \pi/2)$  in the #1 band in Fig. 2(a) shows the character of an  $O_{\parallel} p_{\sigma}$  orbital. This means that an electron is extracted from O<sup>2-</sup> ion in real space, that is, O<sup>2-</sup> ions change to O<sup>1-</sup> ions upon doping holes. As a result, the superexchange interactions between the localized spins via a closed shell of the O<sup>2-</sup> ion in CuO<sub>2</sub> planes are partly destroyed, causing non-AF regions.

Thus, in the insulating phase, the direction of the  $b_{1g}^*$  localized spins becomes random in non-AF regions. Then, a subsequently doped hole entering an upper  $b_{1g}$  orbital at  $(\pi/2, \pi/2)$  forms an SS state with a localized  $b_{1g}^*$  hole by the SS exchange  $K_{b1g}$ . This causes the emergence of a new particle called an SS quasiparticle.

The twisted lines between a  $b_{1g}$  doped hole and a  $b_{1g}^*$  localized hole within the same Cu house (say A-site) in the right side of Fig. 3 represent an entangled coupling produced by SS exchange. This entanglement state at A-site is expressed by the wave function  $\Psi_{ss,A}(\mathbf{r}_1\sigma_1, \mathbf{r}_2\sigma_2)$ , given by

$$\Psi_{ss,A}(\mathbf{r}_1\sigma_1, \mathbf{r}_2\sigma_2) = 1/\sqrt{2} \{ \phi(\mathbf{r}_1 - \mathbf{R}_A) \chi(\mathbf{r}_2 - \mathbf{R}_A) + \phi(\mathbf{r}_2 - \mathbf{R}_A) \chi(\mathbf{r}_1 - \mathbf{R}_A) \} \times 1/\sqrt{2} \{ \alpha(1)\beta(2) - \beta(1)\alpha(2) \} \quad (2)$$

where  $\phi(\mathbf{r})$  and  $\chi(\mathbf{r})$  represent the wavefunctions of the upper  $b_{1g}$  and lower  $b_{1g}^*$  orbitals, respectively. The resonance valence bond (RVB) model [9] and the t-J model [5] also used a similar type of functional form in their theoretical developments.

The entanglement state (SS quasiparticle) hops to a neighboring site B by the transfer interaction ( $H_{tr}$ ) (see Eq. {1} of Ref. [14]). A matrix element of  $H_{tr}$  between neighboring A and B sites ( $\equiv \langle \Psi_{ss,A} | H_{tr} | \Psi_{ss,B} \rangle$ ) takes positive or negative values in a random manner, corresponding to a random spin direction of localized holes in the non-AF region. Thus, an energy level structure of an SS quasiparticle has a feature of a disordered lattice.

When an SS quasiparticle moves in a non-AF region (the right side of Fig. 3), the  $b_{1g}^*$  localized spins (in the first story in this figure) tend to order in a certain sub-region so as to lower the kinetic energy of an SS quasiparticle[17-19]: In one case, the localized spins in a certain sub-region order so that SS quasiparticles may propagate coherently, say, towards the  $x$  direction in that sub-region while in the other case, the localized spins in another sub-region order so that SS quasiparticles can propagate, say, towards the  $-x$  direction.

Following Anderson [20] and Mott [21], these two waves (SS quasiparticles) propagating towards opposite directions may be scattered by a spin-disordered sub-region between the two sub-regions, and interfere with each other, resulting in Anderson-localized states with DOS, which corresponds to the degeneracy representing the number of their localized centers in real space.

When the Fermi energy in a system of SS quasiparticles,  $E_F(\text{SS})$ , increases from the lowest energy in the second Brillouin zone, a particular energy level  $E_c$  appears, where the first Brillouin zone are fully occupied by the  $b_{1g}^*$  localized

holes. This  $E_c$  separates the Anderson-localized states and the extended states in momentum space, and is called a mobility edge, which has a metallic nature. The hole-concentration regime in which  $E_F(\text{SS})$  is below  $E_c$  consists of Anderson-localized states only, and we name this regime an insulating spin-disordered phase. When  $E_F(\text{SS})$  reaches  $E_c$ , the  $b_{1g}$  doped holes (SS quasiparticles) begin to occupy states from  $(\pi/2, \pi/2)$  on the mobility edge. We refer to these metallic states on the mobility edge as a Fermi arc. Thus, the origin of the Fermi arcs we proposed in this paper is different from those based on the t-J model [5, 22, 23].

Now, let us discuss the wavefunction of a hole at  $(\pi, 0)$  in the metallic state, which shows the feature of the KS particles shown in Fig. 1(b). Thus, in the AF region in real space, KS particles emerge at the metal-insulator transition, as shown in the left side of Fig. 3. These KS particles can itinerate in a wider space than the whole AF region, by the spin fluctuation effect in the 2D Heisenberg AF spin system in a  $\text{CuO}_2$  plane. Thus, we can treat the KS particles as carriers in a periodic AF potential. As a result, the KS particles form Fermi pockets (closed Fermi surfaces) around the  $(\pi, 0)$  (antinodal regions) in the second zone in the square (BZ). When this second zone is folded into the AF (BZ), the Fermi pockets appear at the  $\Gamma$  point,  $(0, 0)$ , the center in the AF (BZ).

From the calculated results of Figs. 2(a), 2(b), and 3, a Fermi surface structure of LSCO is constructed. It consists of the Fermi pockets in the antinodal region and Fermi arcs in the nodal region. This Fermi surface structure exhibits the notable doping dependence, whose calculated results are shown in Figs. 4(a), 4(b), and 4(c), which correspond, respectively, to  $x_0 = 0.05$ ,  $x = 0.10$ , and  $x = 0.25$  in the overdoped region, where the temperature is fixed at just above  $T_c$ .

We notice from Figs. 4(a) and 4(b) that, when  $x$  increases from  $x_0 = 0.05$  to  $x_{\text{opm}} = 0.15$ , the portion of Fermi pockets with a 4-pointed petal shape (red and white colors) is expands, together with the expansion of Fermi-arc areas (red line). Here we should also mention that in the 4-pointed petal shape, those within the second (BZ) (red) are hole-like while those in the outside of the second (BZ) (white) are electron-like. Finally, at  $x = 0.25$ , Fermi pockets disappear completely, and thus the Fermi arcs prevail in momentum space, as seen in Fig. 4(c). This means that the character of an  $\text{O}_{\parallel} \text{p}_{\sigma}$  orbital increases with increasing  $x$ , resulting in the partial destruction of superexchange interactions in the local AF order.

This doping dependence of the Fermi surface structure in LSCO is consistent

with that of the electronic entropy in LSCO previously calculated [8, 24], which suggests the phase change from the mixed phase consisting of KS particles and SS quasiparticles in the underdoped region to the pure SS phase consisting of only SS quasiparticles in the overdoped region around  $x = 0.25$ . This theoretical results was supported experimentally by Loram *et al.* [25]. Thus, we call  $x = 0.25$  the critical concentration  $x_c$ ,

We also find that the Fermi surface structure of LSCO exhibits the notable temperature dependences. Since the local AF order is gradually destroyed by thermal agitation when temperature increases, the portion of the KS particles in the mixed phase decreases while the SS quasiparticles in the pure SS phase increases, together with the expansion of non-AF regions. Thus, with increasing temperature, Fermi-pocket regions decrease while Fermi-arc regions increase.

Experimentally, we find that the spectral weight maps in momentum space at  $E_F$  in ARPES experiments of LSCO for  $x = 0.07$  to  $0.22$  [26] are consistent with the calculated Fermi surface structures in Figs. 4(a) to 4(c). The Fermi surface structures of LSCO in Figs. 4(a), 4(b) and 4(c) indicate that the pseudogap in momentum space, previously postulated by Norman, *et al.* [27] has a close relationship to the existence of Fermi pockets. Furthermore, the notable temperature and doping evolutions of the Fermi surface structure in LSCO just clarified explain successfully the unusual behavior of the Fermi surface that has been ascribed to the pseudogap [2, 27, 28].

In this context, a new phase diagram for LSCO is constructed, by introducing the free energies of the mixed phase,  $F_{\text{mix}}(T, x) \equiv E_{\text{mix}}(T, x) - T S_{\text{mix}}(T, x)$  and that of the pure SS phase,  $F_{\text{SS}}(T, x) \equiv E_{\text{SS}}(T, x) - T S_{\text{SS}}(T, x)$ , where  $E(T, x)$  is the internal energy and  $S(T, x)$  is the electronic entropy calculated for LSCO [8, 24]. The thus-constructed phase diagram is shown in Fig. 5, where  $T^*(x)$  is calculated from the equation  $\Delta F(T, x) \equiv F_{\text{mix}}(T, x) - F_{\text{SS}}(T, x) = 0$ . We conclude that  $T^*(x)$  represents the phase change between the mixed phase and the pure SS phase. Thus, at  $x_c$ ,  $T^*(x_c) = 0$ . The order parameter in the mixed phase below  $T^*(x)$  is the spin-correlation length. Since KS particles on the Fermi pockets are responsible for the occurrence of d-wave superconductivity in the phonon mechanism [14, 24], d-wave superconductivity should disappear at  $x = x_c$ , that is  $T_c(x_c) = 0$ . This phase diagram in Fig. 5 is consistent with the following four experimental results:  $T_c(x)$  [29]; the opening of a symmetry gap only in the antinodal region in Bi2212 [30]; the possible existence of antinodal quasiparticles [31]; and the phase diagram for  $\text{Bi}_2\text{Sr}_2\text{CaCu}_2\text{O}_{8+\delta}$  [32].

Finally we discuss the mechanism of superconductivity due to KS particles on the Fermi pockets, following Refs. [14, 24, 33]. Figure 1(b) shows that the wavefunctions of a doped hole with up and down spins,  $\Psi_{k,\uparrow}(\mathbf{r})$  and  $\Psi_{k,\downarrow}(\mathbf{r})$ , have the unique phase relation expressed by  $\Psi_{k,\downarrow}(\mathbf{r}) = \exp(i\mathbf{k} \cdot \mathbf{a}) \Psi_{k,\uparrow}(\mathbf{r})$ , where  $\mathbf{a}$  is a vector representing the Cu-O-Cu distance. Ref. [14] showed that with use of this phase relation, the d-wave superconductivity in the phonon mechanism occurs in LSCO, in the case where Fermi pockets appear at  $(\pi/2, \pi/2)$  in the square (BZ). Since this unique phase relation holds for a the square (BZ) with four-fold symmetry, we can apply the method developed in Ref. [14] to the present case, in which Fermi pockets appear at  $(\pi, 0)$ , as shown below.

Following Ref. [14], the matrix elements of electron-phonon interactions from state  $\mathbf{k}$  to state  $\mathbf{k}'$  of a KS particle with up spin, scattered by a phonon with wave vector  $\mathbf{q}$  in the 2D square AF (BZ),  $V_{\uparrow}(\mathbf{k}, \mathbf{k}', \mathbf{q})$ , have the following spin-dependent property;  $V_{\uparrow}(\mathbf{k}, \mathbf{k}', \mathbf{q}) = \exp(i\mathbf{K} \cdot \mathbf{a}) V_{\downarrow}(\mathbf{k}, \mathbf{k}', \mathbf{q})$ , where  $\mathbf{K} = \mathbf{k} - \mathbf{k}' - \mathbf{q}$  is a reciprocal lattice vector in the 2D square AF (BZ). Here we show that in the case where Fermi pockets appear at  $(\pi, 0)$ , this spin-dependent property also holds. Figure 6 shows that there are the two kinds of scattering processes from states  $\mathbf{k}$  (at **A** point) to  $\mathbf{k}'$  (at **B** point) of a KS particle by a phonon with wave vector  $\mathbf{q}$  in the 2D AF (BZ). A scattering which satisfies  $\mathbf{K} = \mathbf{k} - \mathbf{k}' - \mathbf{q}_n = -\mathbf{Q}_1 - \mathbf{Q}_2$  is a normal scattering, that is,  $\exp(i\mathbf{K} \cdot \mathbf{a}) = +1$  while a scattering which satisfies  $\mathbf{K} = \mathbf{k} - \mathbf{k}' - \mathbf{q}_u = -\mathbf{Q}_2$  is an Umklapp scattering, that is,  $\exp(i\mathbf{K} \cdot \mathbf{a}) = -1$ , where  $\mathbf{a}$  is taken as  $(a, 0)$ , and  $\mathbf{Q}_1$ , and  $\mathbf{Q}_2$  are the AF reciprocal lattice vectors.

Thus, the total effective interaction between states  $\mathbf{k}$  and  $\mathbf{k}'$  of the KS particles for the formation of a Cooper pair which is expressed by the sum of normal and Umklapp scatterings shows the attractive interaction for the normal scattering while the repulsive interaction for the Umklapp scattering in LSCO. Thus, the momentum-dependent electron-phonon spectral function shows the d-wave behavior of  $dx^2 - y^2$ . In this calculation, Fermi arcs are not considered because they are formed by the SS quasiparticles in the non-AF region, and thus do not contribute to superconductivity.

In summary, we have clarified that the Fermi surface structure of LSCO consists of Fermi pockets in the antinodal region and Fermi arcs in the nodal region, and thus that the origin of the pseudogap is the existence of Fermi pockets, and only the KS particles on the Fermi pockets contribute to the phonon mechanism in d-wave superconductivity.

## Acknowledgments

We would like to thank Profs. Atsushi Fujimori, Teppei Yoshida and Kazuyoshi Yamada for their valuable discussion on experimental results and Prof. Dung Hai Lee and Dr. Franco Nori for helpful advice and encouragement regarding the present work. This work was supported by Tokyo University of Science and the Japanese Cabinet-Office-Projects: FIRST and ImPACT.

## References

1. J.G. Bednorz, and K.A Müller, *Z. Phys. B* **64**, 189 (1986).
2. M. R. Norman, D. Pines and C. Kallin, *Adv. Phys.* **54**, 715 (2005)
3. H. Kamimura, S. Matsuno, T. Mizokawa, K. Sasaoka, K. Shiraishi, and H. Ushio, *J. Phys.: Conf. Ser.* **428**, 012043 (2013) and related references therein.
4. C.C. Tsuei, and J.R.Kirtley, *Rev. Mod. Phys.* **72**, 969 (2000).
5. F.C. Zhang, and T.M. Rice, *Phys. Rev. B* **37**, 3759 (1988).
6. D.S. Marshall, D.S. Dessau, A.G. Loese, C.-H. Park, A.Y. Matsuura, J.N. Eckstein, I. Bozovic, P. Fournier, A. Kapitulnik, W.E. Spicer, and Z. -X. Shen, *Phys. Rev. Lett.* **76**, 4841 (1996)
7. H. Kamimura, and Y. Suwa, *J. Phys. Soc. Jpn.* **62**, 3368 (1993).
8. H. Kamimura, T. Hamada, and H. Ushio, *Phys. Rev. B* **66**, 054504 (2002).
9. P.W. Anderson, *Science* **235**, 1196 (1987).
10. See, for example, R.J. Cava, B. Batlogg, S.A. Sunshine, T. Siegrist, H.M. Fleming, K. Rabe, F. Scheemeyer, D.W., Murphy, R.B. van Dover, P.K. Gallagher, S.H. Clarum, S. Nakayama, R.C. Farrow, J.J. Krajewski, S.R. Zahurak, J.V. Waszak, J.H. Marshall, P. Marsh, L.W. Jr. Rupp, W.F. Peck, and E.A. Rietman, *Physica C* **153-155**, 560 (1988).
11. C.T. Chen, L.H. Tjeng,, Kwo, H. L. Kao, P. Rudolf, P. Sette, R.M. Fleming, *Phys. Rev. Lett.* **68**, 2543 (1992).
12. E. Pellegrin, N. Nücker, J. Fink, S.L. Molodtsov, A. Gutierrez, E. Navas, O. Sterebel, Z. Hu, M. Domke, G. Kaindl, S. Uchida, Y. Nakamura, J. Marki, M. Klaude, G. Saemann=Ischenko, A. Krol, JL. Peng, Z.Y. Li, R.L. Greene, *Phys. Rev. B* **47**, 3354 (1993)
13. V.L. Anisimov, S.Y. Ezhov, and T.M. Rice, *Phys. Rev. B* **55**, 12829 (1997).
14. H. Kamimura, S. Matsuno, Y. Suwa, and H. Ushio, *Phys. Rev. Lett.* **77**, 723 (1996).
15. M. Eto and H. Kamimura, *J. Phys. Soc. Jpn.* **60**, 2311 (1991); and related references therein.
16. H. Ushio and H Kamimura, *J. Phys. Soc. Jpn.* **64**, 2585 (1995).
17. T. Hamada, K. Ishida, H. Kamimura, and Y. Suwa, *J. Phys. Soc. Jpn.* **70**, 2033 (2001).

18. K. Yamada, C.H. Lee, K. Kurahashi, J. Wada, S. Wakimoto, S., Ueki, H. Kimura, and Y. Endoh, Phys. Rev. B **57**, 6165 (1998).
19. P. Wrobel, R. Eder and P. Fulde, J. Phys. : Condens. Matter, **15**, 6599 (2003), and related references therein.
20. P.W Anderson, Phys. Rev. **109**, 35 (1958)
21. N.F. Mott, *Conduction in Non-Crystalline Materials*. (Oxford University Press, New York, 1987) and related references therein.
22. K.-Y. Yang, T.Y. Rice and F.-C. Zhang, Phys. Rev. B **73**, 174501 (2006); and related references therein.
23. T.J. Reber, N.C. Plumb, Z. Sun, Y. Gao, Q. Wang, K. McElroy, H. Iwasawa, M. Arita, J.S. Wen,, Z.J. Xu, G. Gu, Y. Yoshida, H. Eisaki, Y. Aiura, and D.S. Dessau, Nature Phys. **8**, 606 (2012); and related references therein.
24. H. Kamimura, T. Hamada, S. Matsuno and H. Ushio, Physica C **364-365**, 87 (2001)
25. J.W. Loram, K.A. Mirza, J.R. Cooper, and J.L. Tallon, J. Phys. Chem. Solids **59**, 2091 (1998).
26. T. Yoshida, X.J. Zhou, K. Tanaka, W.L Yang, Z. Hussain, Z.-X. Shen, A. Fujimori, S. Sahrakorpi, M. Lindroos, R.S. Markiewicz, A. Bansil, , S. Komiya, Y. Ando, H. Eisaki, T. Kakeshita, , and S. Uchida, Phys. Rev. B **74**, 224510 (2006).
27. M.R. Norman, H. Ding, M. Randeriat, J.C. Campuzano,, T. Yokoya, T. Takeuchi, T., Takahashi, T., Mochiku, T. Kadokawa, K. Guptasarma, and D.G.Hinks, Nature **392**, 157 (1998).
28. A. Kanigel, M.R. Norman, M. Randeria, U. Chatterjee, S. Souma, A. Kaminski, H.M. Fretwell, D. Hinks, L, Ozyuzer, J.C. Camuzano, Nature Physics **2**, 447 (2006)
29. H. Takagi, T. Ido, S. Ishibashi, M. Uota, S. Uchida, Y. Tokura, Phys. Rev. B **40**, 2254 (1989).
30. H.-B. Yang, J.D. Rameau, P.D. Johnson, T. Valla, A. Tsvelik, G.D. Gu,: Nature **456**, 77 (2008)
31. K. McElroy, R.W. Simmonds, J.R. Hoffman, D.-H. Lee, J. Orenstein, H. Eisaki, S. Uchida, and J.C. Davis, Nature **422**, 592 (2003).
32. I.M. Vishik, M. Hashimoto, R.-H. He, W.-S. Lee, F. Schmitt, D. Lu, B.G. Moore, C. Zhang, W. Meevasana, T. Sasagawa, S. Uchida, K. Fujita, S. Ishida, M. Ishikado, Y. Yoshida, H. Eisaki, Z. Hussain, P.

Thomas, T.P. Devoreaux, and Z.-X. Shen, Proc. Natl. Acad. Sci. USA **109**, 18332 (2012).

33. H. Kamimura, T. Hamada, S. Matsuno and H. Ushio, J. Supercond. **15**, 379 (2002)

Fig1

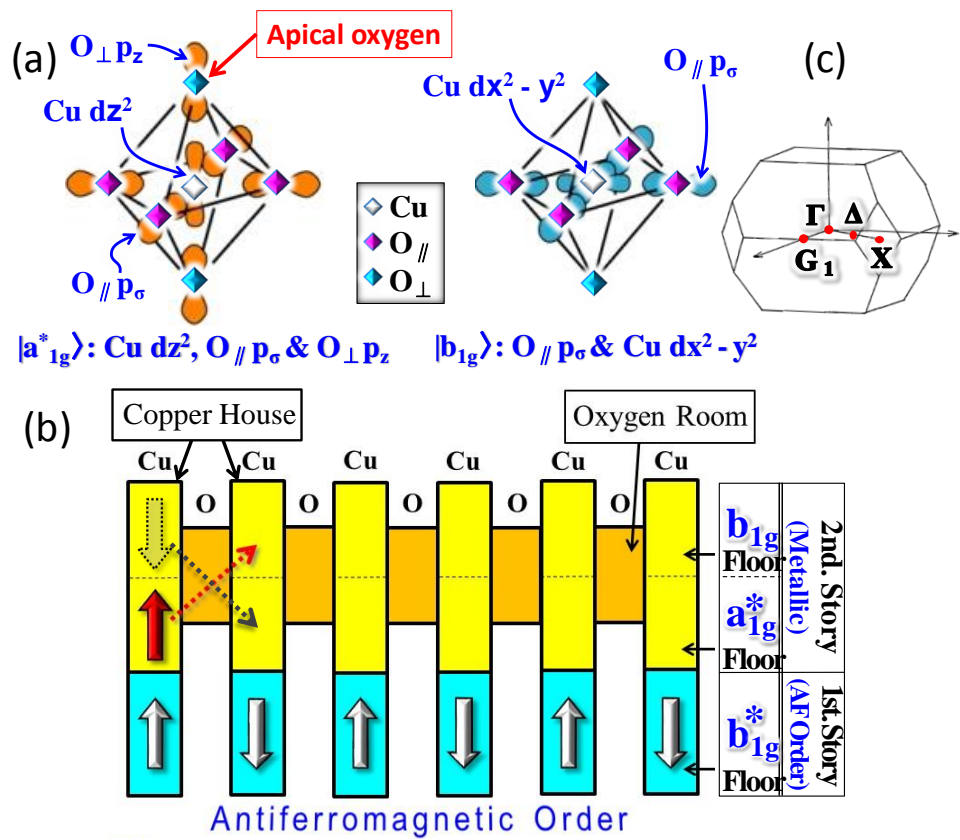


Fig2

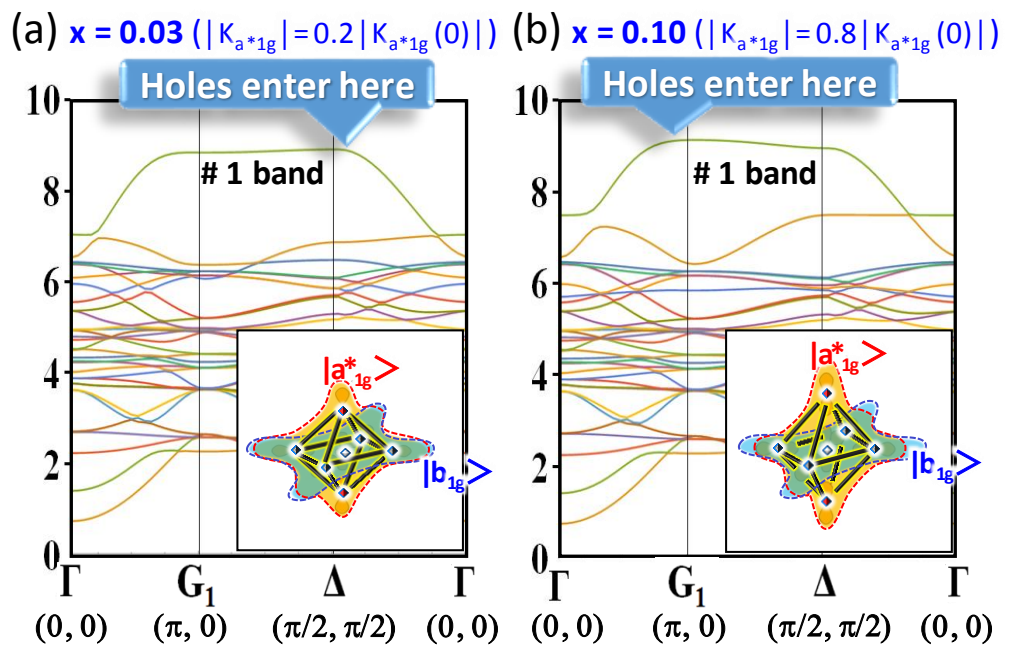


Fig3

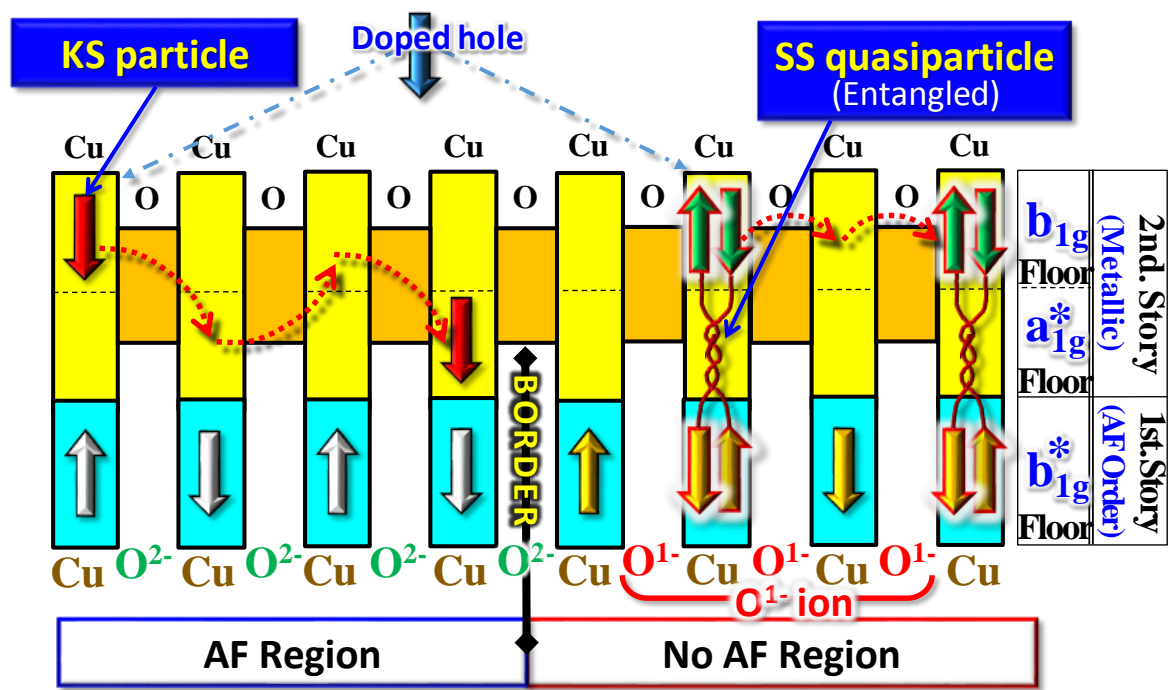


Fig4

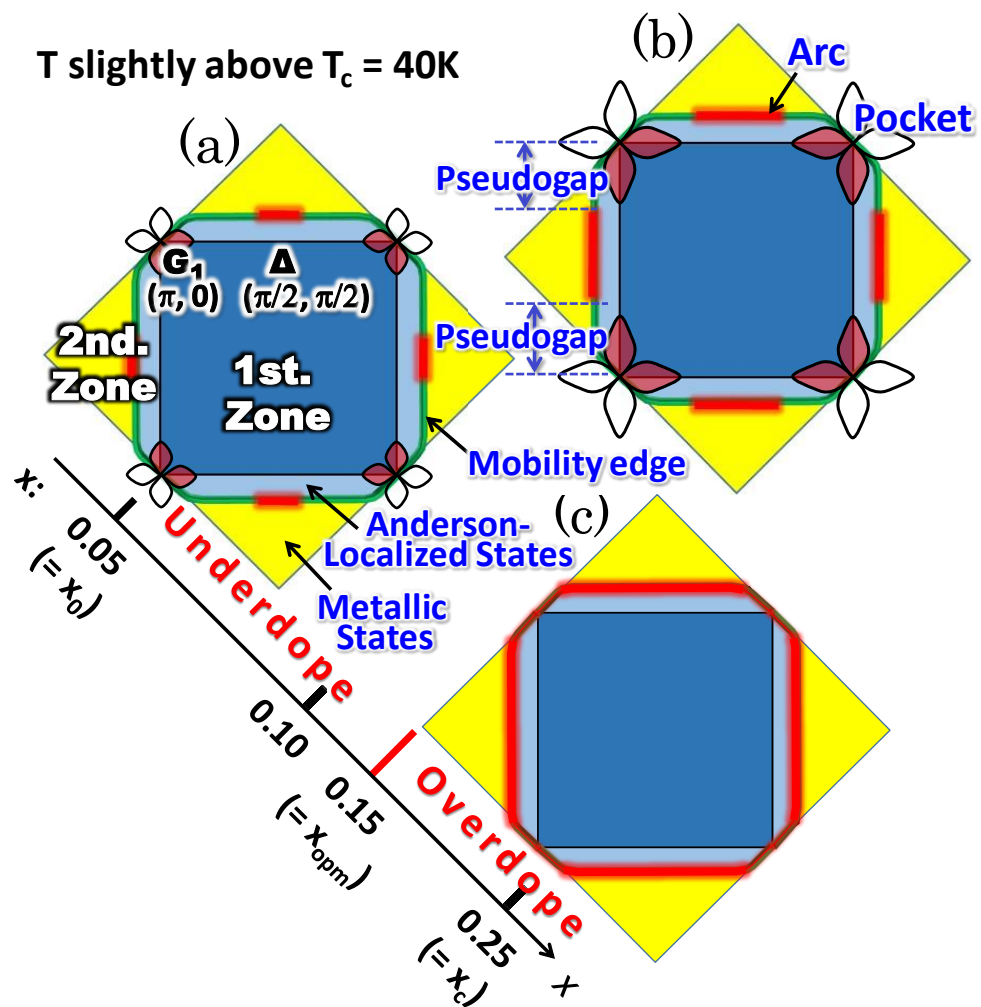


Fig5

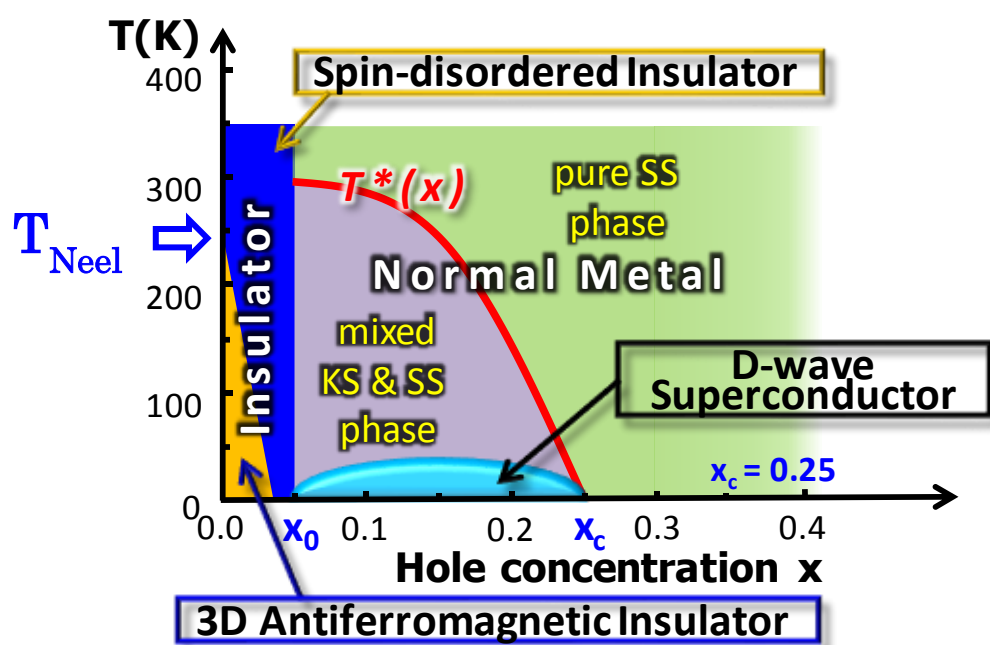
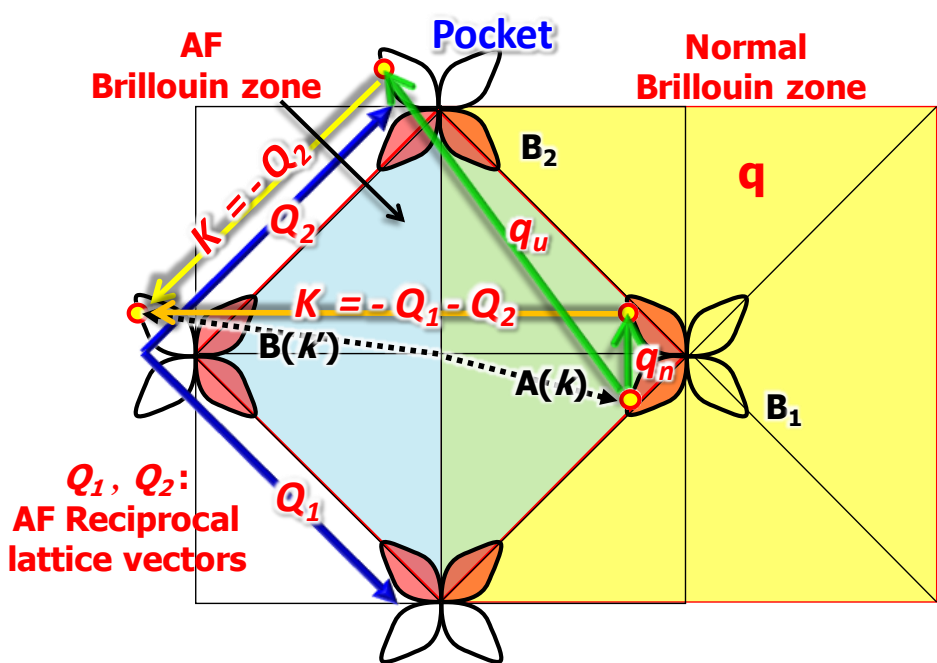


Fig6



## **Figure captions**

**Figure 1.(Color online)** Relevant electronic orbitals and a heuristic explanation of the K-S model

**(a)** Sketch of  $|a_{1g}^* \rangle$  and  $|b_{1g} \rangle$  orbitals. **(b)** The extended two-story house model. The first story is occupied by  $b_{1g}^*$  localized spins while a doped hole (a KS particle) with up spin (red arrow) or with down spin (black dotted arrow) enters the second story which consists of lower  $a_{1g}^*$  and upper  $b_{1g}$  floors. **(c)** Ordinary Brillouin zone of LSCO with  $\Gamma$ ,  $\Delta$ ,  $G_1$  and  $X$  symmetry points..

**Figure 2. (Color online)** Notable change of the energy bands for LSCO upon doping holes. **(a)** Band structure for  $x = 0.03$ . Inset sketches a small overlap, resulting in  $|K_{a^*1g}| = 0.2 |K_{a^*1g}(0)|$ , where  $|K_{a^*1g}(0)| = 2.0$  eV. **(b)** Band structure for  $x = 0.10$ . Inset shows a large overlap, resulting in  $|K_{a^*1g}| = 0.8 |K_{a^*1g}(0)|$ .

**Figure 3. (Color online)** Emergence of an SS quasiparticle in the non-AF region (right side) and that of a KS particle in the AF region (left side)

**Figure 4. (Color online)** Fermi surface structure of LSCO and its notable doping dependence, where the mobility edge, Fermi arcs and Fermi pockets are shown, respectively, by green color lines, red lines and red-white 4-pointed petal shapes, respectively.  $x = 0.05$ . **(b)**  $x = 0.10$ . **(c)**  $x_c = 0.25$ .

**Figure 5. (Color online)** New phase diagram,  $T$  vs  $x$  for LSCO.

**Figure 6. (Color online)** Verification of d-wave superconductivity. Illustration of two scattering processes by phonons: Normal and Umklapp.